

# The vertical and spatial structure of ENSO in the upper troposphere and lower stratosphere from GPS radio occultation measurements

B. Scherllin-Pirscher,<sup>1,2</sup> C. Deser,<sup>3</sup> S.-P. Ho,<sup>2</sup> C. Chou,<sup>4</sup> W. Randel,<sup>3</sup> and Y.-H. Kuo<sup>2</sup>

Received 12 July 2012; revised 3 September 2012; accepted 5 September 2012; published 17 October 2012.

[1] The vertical and spatial structure of the atmospheric El Niño-Southern Oscillation (ENSO) signal is investigated using radio occultation (RO) data from August 2006 to December 2010. Due to their high vertical resolution and global coverage, RO data are well suited to describe the full 3-dimensional ENSO structure in the troposphere and lower stratosphere. We find that interannual temperature anomalies in the equatorial region show a natural decomposition into zonal-mean and eddy (deviations from the zonal-mean) components that are both related to ENSO. Consistent with previous studies, we find that during the warm phase of ENSO, zonal-mean temperatures increase in the tropical troposphere and decrease in the tropical stratosphere. Maximum warming occurs above 8 km, and the transition between warming and cooling occurs near the tropopause. This zonal-mean response lags sea surface temperature anomalies in the eastern equatorial Pacific by 3 months. The atmospheric eddy component, in contrast, responds rapidly (within 1 month) to ENSO forcing. This signal features a low-latitude dipole between the Indian and Pacific Oceans, with off-equatorial maxima centered around 20° to 30° latitude in both hemispheres. The eddy response pattern attains maximum amplitude in the upper troposphere near 11 km and (with opposite polarity) in a shallow layer near the tropopause at approximately 17 km. The eddy ENSO signal tends to be out-of-phase between low and middle latitudes in both the troposphere and lower stratosphere. **Citation:** Scherllin-Pirscher, B., C. Deser, S.-P. Ho, C. Chou, W. Randel, and Y.-H. Kuo (2012), The vertical and spatial structure of ENSO in the upper troposphere and lower stratosphere from GPS radio occultation measurements, *Geophys. Res. Lett.*, 39, L20801, doi:10.1029/2012GL053071.

## 1. Introduction

[2] Global weather and climate are influenced by the interannual El Niño-Southern Oscillation (ENSO) phenomenon, which emerges from atmosphere-ocean interaction in the tropical Pacific. Atmospheric temperature variations

<sup>1</sup>Wegener Center for Climate and Global Change and Institute for Geophysics, Astrophysics, and Meteorology/Institute of Physics, University of Graz, Graz, Austria.

<sup>2</sup>COSMIC Project Office, University Corporation for Atmospheric Research, Boulder, Colorado, USA.

<sup>3</sup>National Center for Atmospheric Research, Boulder, Colorado, USA.

<sup>4</sup>Research Center for Environmental Changes, Academia Sinica, Taipei, Taiwan.

Corresponding author: B. Scherllin-Pirscher, Wegener Center for Climate and Global Change, University of Graz, Brandhofgasse 5, A-8010 Graz, Austria. (barbara.pirscher@uni-graz.at)

associated with ENSO are pronounced not only at low latitudes within the troposphere, but also at middle and high latitudes as well as in the stratosphere [e.g., Seager *et al.*, 2003; Free and Seidel, 2009; Randel *et al.*, 2009].

[3] The warm phase of ENSO is associated with tropospheric warming, which is attributable to anomalous heat flux from the tropical Pacific ocean to the atmosphere [Seager *et al.*, 2003] and is a well-known feature of interannual tropical temperature variability. Relative to the sea surface temperature (SST) forcing in the eastern equatorial Pacific, this tropospheric response is lagged by one or two seasons [Su *et al.*, 2005; Chou and Lo, 2007]. In the lower tropical stratosphere, a significant cooling signal is linked to the warm phase of ENSO [Lau *et al.*, 1998; Free and Seidel, 2009], produced by enhanced tropical upwelling [Randel *et al.*, 2009; Calvo *et al.*, 2010]. Modeling studies confirm the existence of this stratospheric cooling signal [García-Herrera *et al.*, 2006].

[4] Using observations from the Microwave Sounding Unit (MSU), Yulaeva and Wallace [1994] and Calvo Fernández *et al.* [2004] found different ENSO signatures for the zonal-mean and eddy (deviations from the zonal-mean) temperature components within the upper troposphere and lower stratosphere. However, since MSU provides information only for thick (>10 km) atmospheric layers these studies were unable to extract the detailed vertical structure of the zonal-mean and eddy ENSO signals.

[5] Trenberth and Smith [2006, 2009] and Zhou and Zhang [2011] used global reanalysis and model data to analyze the full 3-dimensional temperature structure associated with ENSO. They identified two distinctive modes which together capture the full character of the atmospheric ENSO signal. These two patterns and their corresponding time-series are in general agreement with the observed vertical structures of the zonal-mean and eddy ENSO signals obtained from the coarse-resolution MSU data [Yulaeva and Wallace, 1994; Calvo Fernández *et al.*, 2004].

[6] Building upon these previous studies, we analyze the full vertical and spatial structure of the ENSO signal in atmospheric temperatures within the troposphere and lower stratosphere up to 20 km using Global Positioning System (GPS) radio occultation (RO) data. The unprecedented vertical resolution and global coverage of the RO data provide a more detailed view of the full 3-dimensional ENSO structure than other observational data sets. Early studies of ENSO using RO data have been performed in the framework of climate change detection studies [Steiner *et al.*, 2011].

## 2. Data and Methods

[7] We use RO temperature and water vapor pressure profiles from three satellite missions: CHALLENGING Mini-

Satellite Payload (CHAMP), Formosa Satellite Mission 3/ Constellation Observing System for Meteorology, Ionosphere, and Climate (FORMOSAT-3/COSMIC, F3C), and Gravity Recovery And Climate Experiment (GRACE) (for a review on RO missions and data applications, see *Anthes* [2011]). We use data for the period August 2006 to December 2010 when there are more than 40000 profiles in a month. During this period warm ENSO (El Niño) events occurred in 2006/2007 and 2009/2010 and cold ENSO (La Niña) events in 2007/2008 and at the end of 2010. Neutral ENSO conditions were observed in 2008/2009. We formed monthly averages of all profiles which passed the processing center's quality control procedures, and gridded them into  $5^\circ$  latitude by  $5^\circ$  longitude boxes and a vertical resolution of 100 m. If no profiles were available for a particular  $5^\circ \times 5^\circ$  grid box, we bi-linearly interpolated the profiles from neighboring grid-cells to fill the missing data. Due to the strong confounding effects of the Quasi Biennial Oscillation (QBO) and ENSO in the short RO record, we only use RO temperature profiles below 20 km.

[8] In humid regions (i.e., in the lower troposphere), a priori knowledge of the state of the atmosphere is needed to derive temperature and water vapor from RO measurements. Since lower tropospheric temperature can be significantly affected by the background data, we focus the interpretation of our results on the upper troposphere and lower stratosphere region. Total column water vapor, which is derived from RO water vapor pressure profiles, was found to be consistent with those from ground-based GPS observations and those from ECMWF [e.g., *Ho et al.*, 2010].

[9] Monthly mean anomalies are obtained from subtracting the mean annual cycle at each grid point. The latter is calculated from January 2007 to December 2010. The monthly anomalies were then smoothed with a 3-point binomial (1-2-1) filter to reduce month-to-month variations.

[10] We apply Principal Component Analysis (PCA) and multiple linear regression analysis to identify the ENSO signal. For multiple linear regression, we regress monthly temperature anomalies against the monthly Niño 3.4 (N3.4) SST index (the N3.4 region ranges from  $5^\circ\text{S}$  to  $5^\circ\text{N}$  and  $120^\circ\text{W}$  to  $170^\circ\text{W}$ ) provided by the NOAA Climate Prediction Center, and against the first and second principal components (PCs) of Singapore zonal winds [*Wallace et al.*, 1993], which serve as proxies for QBO variability. QBO regression is important in the lower stratosphere because the signal penetrates below 20 km. N3.4 and QBO indices are also smoothed with a 1-2-1 filter prior to the regression analysis.

[11] Uncertainty estimates for the regression coefficients are calculated using a bootstrap resampling technique but we did not account for field significance, which tests the pattern itself. This may overestimate significance in regions, where features are only marginally significant. The statistical significance of the correlations is assessed by applying a Student's *t*-test at the 95% confidence level and accounting for autocorrelations [see *Oort and Yienger*, 1996].

### 3. Results

[12] Figure 1 shows results for the equatorial plane based on averages from  $5^\circ\text{S}$  to  $5^\circ\text{N}$ . Interannual temperature variability, given by the standard deviation field, is largest above the tropopause across all longitudes ( $>1.5$  K), and is

attributable to the QBO. High variability ( $>1.0$  K) also occurs in the upper troposphere (7 km to 13 km) in the longitude sector  $90^\circ\text{W}$  to the date line. This sector corresponds approximately to the N3.4 region where SST variations associated with ENSO are largest.

[13] The dominant pattern of interannual equatorial temperature variability in the longitude-height plane, given by the leading empirical orthogonal function (EOF1), exhibits a zonally-symmetric structure of warming within the troposphere (maximum values at upper levels) and cooling within the lower stratosphere (Figure 1b). In addition, there is a pronounced zonally-asymmetric signal over the N3.4 longitudinal sector with maximum warming ( $>1$  K) between 8 km and 12 km and stratospheric cooling that penetrates below the tropopause. This EOF is closely associated with ENSO: the correlation coefficient between its corresponding PC time series and the N3.4 index is 0.79 at a lag of 3 months.

[14] Given the natural split of EOF1 into zonally symmetric and asymmetric components, we apply EOF analysis to each component separately following *Calvo Fernández et al.* [2004]. EOF1 of the zonal-mean temperature anomaly field shows tropospheric warming and stratospheric cooling, with the nodal line at the altitude of the climatological tropopause (16.5 km) (Figure 1c). This vertical profile reflects the quasi-moist adiabatic behavior of the tropical atmosphere. On the other hand, EOF1 of the eddy field shows maximum amplitude over the N3.4 longitudinal sector, with warming below 14 km and maximum cooling at and directly above the tropopause (17 km to 18 km; Figure 1d). The corresponding PC time series are again highly correlated with the N3.4 index:  $r = 0.75$  for the zonal-mean PC1 at a lag of 3 months and  $r = 0.93$  for the eddy PC1 at zero lag.

[15] Figures 1e and 1f show the temporal evolutions of zonal-mean temperature anomalies and eddy temperature anomalies averaged across the N3.4 longitudinal sector, respectively. Both records reveal positive temperature anomalies during El Niño conditions and negative anomalies during La Niña conditions. Above the tropopause, the zonally-symmetric QBO phenomenon dominates the zonal-mean field. Consistent with the EOF results, the zonal-mean temperature anomalies lag the eddy anomalies by several months and exhibit a different vertical structure, with the transition between positive and negative anomalies occurring near the tropopause in the zonal-mean field and at approximately 14 km altitude in the eddy field.

[16] We further analyze the interannual temperature variability by applying a separate PCA to each altitude level for both the zonal-mean and eddy anomaly fields over the latitude-longitude domain  $30^\circ\text{S}$  to  $30^\circ\text{N}$  and  $0^\circ$  to  $360^\circ\text{E}$ . The leading EOF at each altitude is associated with ENSO, as shown by the correlation and regression coefficients between the corresponding PC time series and the N3.4 index at the lag at which these coefficients are maximized (Figures 1g and 1h, respectively). The correlations are generally positive in the troposphere, where they exceed 0.8, and negative in the stratosphere where they are less than  $-0.9$  ( $-0.6$ ) for the eddy (zonal-mean) component. Due to the QBO signal, zonal-mean correlations are lower (but still statistically significant) in the lower stratosphere. Consistent with the results shown in Figure 1 (top panels), the transition between positive and negative values is more abrupt and occurs at a lower altitude (approximately 14 km compared to 17 km) in the eddy field than the zonal-mean field. Due to

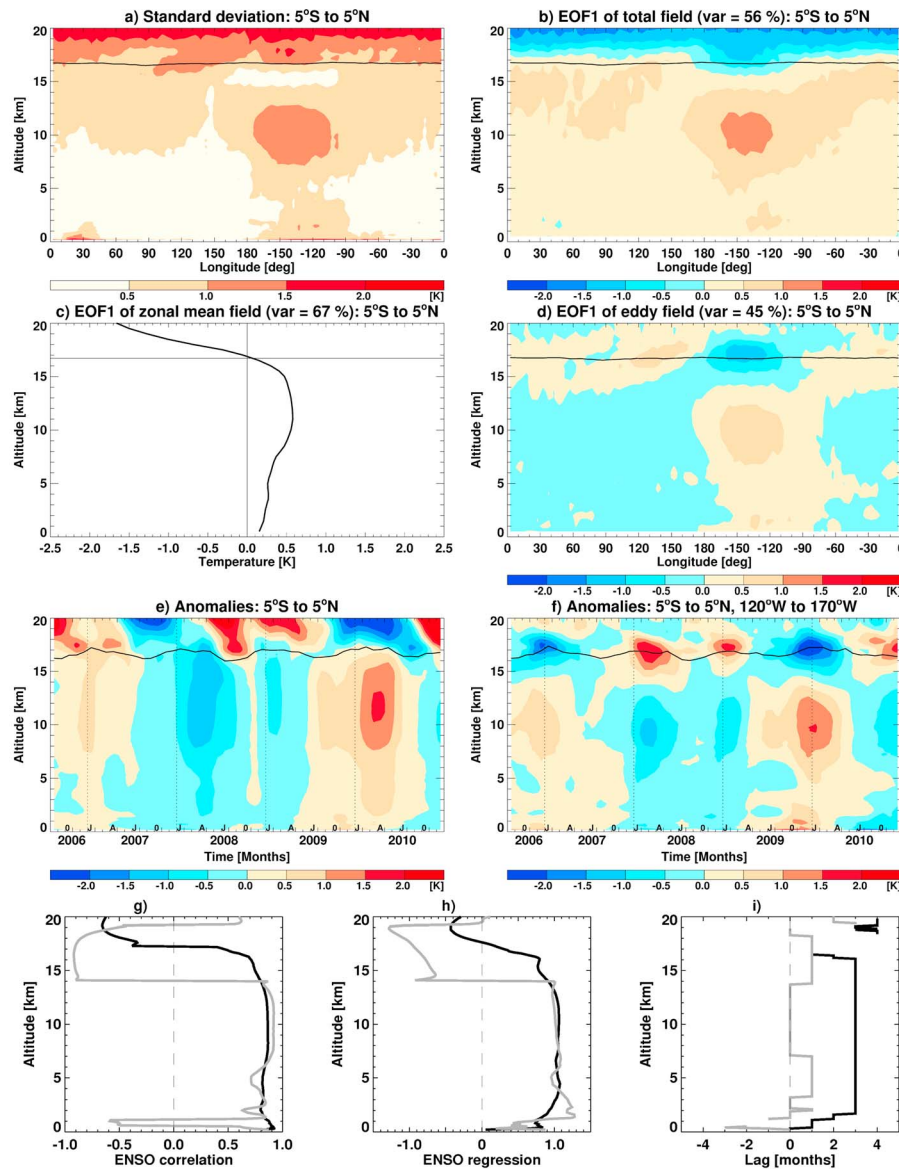


**Figure 1.** Zonal cross sections from 5°S to 5°N of (a) deseasonalized temperature standard deviation, (b) EOF1 of the temperature anomaly field, (c) EOF1 of the zonal-mean field, and (d) EOF1 of the eddy field. Temporal evolutions of (e) zonal-mean temperature anomaly between 5°S and 5°N and (f) eddy temperature anomaly calculated in the N3.4 region. In each panel, the lapse-rate tropopause altitude is shown for reference (black curves). Vertical profiles shown in Figures 1g–1i are based on a separate PC analysis over the 30°S to 30°N, 0° to 360°E domain calculated at each altitude level separately. (g) Correlation between zonal-mean/eddy PC1 and the N3.4 index at the lag at which these coefficients are maximized, (h) regression coefficients obtained from regressing zonal-mean/eddy PC1 onto the N3.4 index, and (i) lag (in months) where the maximum correlation (shown in Figure 1g) is obtained. Zonal-mean results are shown in black, eddy results in gray. ENSO lag (Figure 1i) is only plotted if correlations are statistically significant.

the short record, correlations smaller than approximately 0.6 in absolute value are not statistically significant.

[17] The lag at which the correlation/regression coefficient is maximized occurs consistently at approximately 3 months for PC1 of the zonal-mean field and 0 to 1 month for PC1 of the eddy field across a wide range of altitudes (Figure 1i), in good agreement with the results of *Yulaeva and Wallace [1994]* and *Calvo Fernández et al. [2004]*. The 3-month lag for the zonal-mean field can be attributed to exchange of fluxes at the atmosphere–ocean interface and the atmospheric energy loss to space and to mid latitudes [*Su et al., 2005*].

The fast response of the eddy ENSO signal is related to local heating induced by positive SST anomalies. Vertically propagating Kelvin waves induce a rapid response of the tropical troposphere to an anomalous diabatic heat source [*Ryu et al., 2008*].

[18] Regression maps of the zonal-mean and eddy temperature anomaly fields in the lower stratosphere (16 km to 17 km) and upper troposphere (9 km to 10 km) upon the N3.4 index are shown in Figures 2a and 2b, respectively. We used a lag of 3 months for the zonal-mean field and zero lag for the eddy field, using multiple linear regression analysis

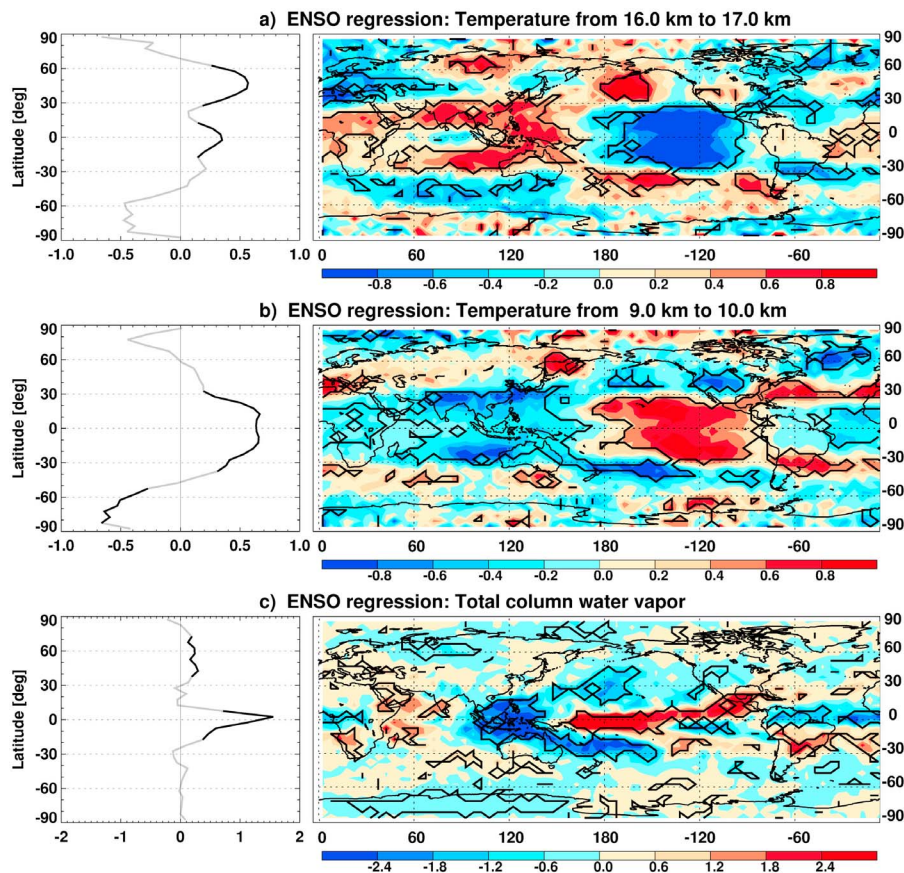


**Figure 2.** ENSO regression coefficients of the (left) zonal-mean and (right) eddy temperature fields in the altitude layer from (a) 16 km to 17 km and (b) 9 km to 10 km. (c) ENSO regression coefficients of total column water vapor fields. Solid black lines enclose areas of statistically significant regressions.

that includes the two QBO terms. Similar results are obtained using the zonal-mean/eddy PC1 time-series in place of the N3.4 index with appropriate lag (not shown). As a measure of diabatic forcing of these temperature patterns, we also show the corresponding regression maps of total column water vapor in Figure 2c.

[19] The zonal-mean regression maps (Figure 2, left) show a narrow equatorial peak in total column water vapor, which is accompanied by a broad tropical ( $30^{\circ}\text{S}$  to  $30^{\circ}\text{N}$ ) temperature maximum in the upper troposphere and lower stratosphere. Negative temperature anomalies are also evident over southern high latitudes ( $50^{\circ}\text{S}$  to  $80^{\circ}\text{S}$ ) at both altitude levels, although only the values at 9 km to 10 km are statistically significant. An additional temperature maximum is found over northern middle latitudes ( $30^{\circ}\text{N}$  to  $60^{\circ}\text{N}$ ) in the lower stratosphere.

[20] The eddy regression maps feature a narrow equatorial maximum over the central Pacific surrounded by negative values over the maritime continent, the South Pacific Convergence Zone (SPCZ), and the subtropical North Pacific. Additional signals are evident over the tropical Atlantic and eastern Pacific. The corresponding temperature pattern at low latitudes is symmetric about the equator and shows an east-west Indo-Pacific dipole centered slightly west of the date line, with off-equatorial maxima centered around  $20^{\circ}$  to  $30^{\circ}$  in both hemispheres. This dipole reverses polarity between the tropical middle troposphere (9 km to 10 km layer) and tropical upper troposphere (16 km to 17 km

layer). This pattern has also been observed by *Yulaeva and Wallace* [1994], *Lau et al.* [1998], *Randel et al.* [2000], and *Calvo Fernández et al.* [2004]. Idealized model calculations suggest that such a pattern is associated with Rossby and Kelvin circulations induced by equatorial heating anomalies [*Gill*, 1980; *Highwood and Hoskins*, 1998].

[21] The latitude-height cross section of the zonal-mean temperature regression coefficients (Figure 3a) shows several statistically significant features including: warming throughout the tropical troposphere with maximum amplitudes above 8 km; warming of the northern high latitude troposphere with maximum values at  $70^{\circ}\text{N}$  to  $80^{\circ}\text{N}$ ; cooling in the lower stratosphere (10 km to 17 km) at southern high latitudes ( $50^{\circ}\text{S}$  to  $85^{\circ}\text{S}$ ), some of which penetrates down into the troposphere; and a stratospheric dipole pattern of negative anomalies in the deep tropics ( $10^{\circ}\text{N}$  to  $10^{\circ}\text{S}$ ), and positive anomalies at northern middle latitudes ( $30^{\circ}\text{N}$  to  $60^{\circ}\text{N}$ ) with maximum amplitude near the upper boundary of our domain (20 km). With exception of the southern high latitude cooling and the strength of the tropospheric northern high latitude warming, these features have also been found in other studies, e.g., by *Seager et al.* [2003], *Lu et al.* [2008], *Free and Seidel* [2009], *Randel et al.* [2009], and *Calvo et al.* [2010]. The southern high latitude signal just might be representative for the period from 2006 to 2010.

[22] Meridional cross sections of the eddy temperature regression coefficients over the maritime continent ( $110^{\circ}\text{E}$  to  $130^{\circ}\text{E}$ ) and central Pacific ( $140^{\circ}\text{W}$  to  $160^{\circ}\text{W}$ ) reveal

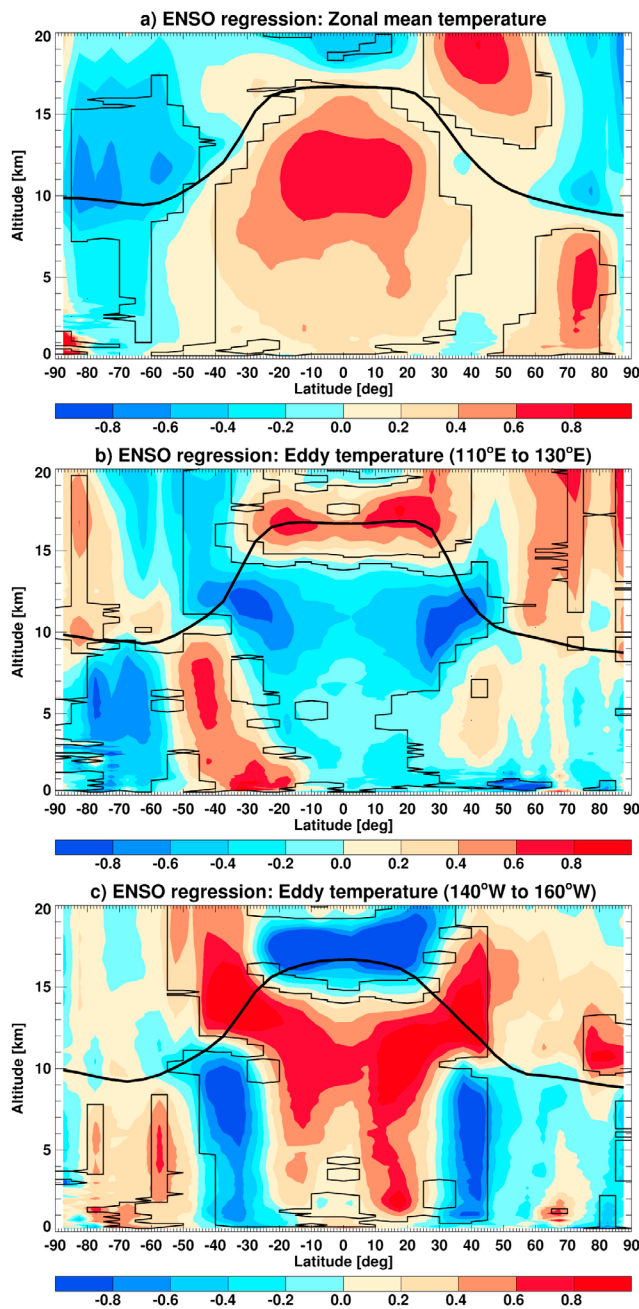


**Figure 3.** Meridional cross sections of ENSO regression coefficients of (a) zonal-mean temperature, eddy temperature centered at (b)  $120^{\circ}\text{E}$ , and (c)  $150^{\circ}\text{W}$ . Thin solid black lines enclose areas of statistically significant regressions. Thick black lines denote the mean lapse-rate tropopause altitude.

similar structures with opposite polarity (Figures 3b and 3c). Taking the central Pacific perspective, off-equatorial ( $10^{\circ}$  to  $20^{\circ}$ ) maxima are coupled with mid-latitude ( $30^{\circ}$  to  $50^{\circ}$ ) minima within the troposphere of both hemispheres. These signals are generally weaker over the maritime continent compared to the central Pacific, especially within the lower troposphere. In addition to these tropospheric responses, negative (positive) temperature anomalies centered at the tropopause are found within the tropics (middle latitudes)

over the central Pacific. Similar features with opposite sign and weaker amplitude are found over the maritime continent. Using a linearized Boussinesq model, *Holloway and Neelin* [2007] show that a shallow layer of cooling occurs close to the tropopause in conjunction with tropical tropospheric heating. They suggest that this cooling layer results from hydrostatic horizontal pressure gradients that extend above the top of the convective heating and cause divergence and adiabatic ascent.

#### 4. Summary

[23] We have used radio occultation (RO) data to investigate the vertical and spatial structure of global atmospheric temperature anomalies associated with ENSO in the troposphere and lower stratosphere. Despite the relatively short record, we were able to demonstrate that the RO data clearly capture the ENSO signal.

[24] Interannual temperature anomalies in the equatorial region show a natural decomposition into zonal-mean and eddy components, both of which are related to ENSO. While the zonal-mean component lags sea surface temperature (SST) anomalies in the eastern equatorial Pacific ( $\text{N}3.4$  region) by 3 months, the eddy component responds rapidly (within 1 month). These results are consistent with those of previous studies and known mechanisms, as discussed above.

[25] The unprecedented vertical resolution of the RO data provided a detailed view of the full 3-dimensional ENSO structure. During the warm phase of ENSO, zonal-mean temperatures increase in the tropical troposphere and decrease in the tropical stratosphere. High-resolution RO data clearly show that maximum warming occurs above 8 km, and that the transition between warming and cooling occurs near the tropopause.

[26] The atmospheric eddy ENSO signal features an Indo-Pacific dipole at low latitudes, with off-equatorial maxima centered around  $20^{\circ}$  to  $30^{\circ}$  latitude in both hemispheres. This pattern has also been found in previous studies and is consistent with Rossby and Kelvin wave circulations induced by equatorial heating anomalies [*Gill*, 1980; *Highwood and Hoskins*, 1998]. However, the high-resolution RO data reveal the detailed vertical structure of this pattern, which attains maximum amplitude in the upper troposphere near 11 km and (with opposite polarity) in a shallow layer near the tropopause at approximately 17 km. The shallow response near the tropopause has been shown to result from hydrostatic horizontal pressure gradients associated with deep convective heating as modeled by *Holloway and Neelin* [2007]. At mid latitudes, eddy ENSO signals are out-of-phase with those at low latitudes.

[27] So far, a sufficient number of RO measurements is available only for a few ENSO cycles. A follow-on multi-satellite RO mission, currently in the planning stage, will provide a longer RO record, which will enable a better separation of the ENSO and QBO signals in the lower stratosphere, and allow for a more robust assessment of the detailed vertical and spatial structures of interannual temperature variability.

[28] **Acknowledgments.** We would like to acknowledge UCAR/CDAAC, Boulder, CO, USA, for the provision of RO data products. Furthermore, we want to thank CPC for providing the  $\text{N}3.4$  index, and Barbara Naujokat for Singapore zonal winds. The study was funded by the Austrian

Science Fund (FWF) under research grant P22293-N21 (BENCHCLIM) and the National Science Foundation under Cooperative Agreement AGS-0918398/CSA AGS-0939962. The National Center for Atmospheric Research is sponsored by the National Science Foundation.

[29] The Editor thanks the two anonymous reviewers for assisting in the evaluation of this paper.

## References

- Anthes, R. A. (2011), Exploring Earth's atmosphere with radio occultation: Contributions to weather, climate, and space weather, *Atmos. Meas. Tech.*, *4*, 1077–1103, doi:10.5194/amt-4-1077-2011.
- Calvo, N., R. R. Garcia, W. J. Randel, and D. R. Marsh (2010), Dynamical mechanism for the increase in tropical upwelling in the lowermost tropical stratosphere during warm ENSO events, *J. Atmos. Sci.*, *67*, 2331–2340, doi:10.1175/2010JAS3433.1.
- Calvo Fernández, N., R. R. Garcia, R. Garcia Herrera, D. Gallego Puyol, L. G. Presa, E. Hernández Martín, and P. Ribera Rodríguez (2004), Analysis of the ENSO signal in tropospheric and stratospheric temperatures observed by MSU, 1979–2000, *J. Clim.*, *17*(20), 3934–3946.
- Chou, C., and M.-H. Lo (2007), Asymmetric responses of tropical precipitation during ENSO, *J. Clim.*, *20*, 3411–3433, doi:10.1175/JCLI4197.1.
- Free, M., and D. J. Seidel (2009), Observed El Niño–Southern Oscillation temperature signal in the stratosphere, *J. Geophys. Res.*, *114*, D23108, doi:10.1029/2009JD012420.
- García-Herrera, R., N. Calvo, R. R. Garcia, and M. A. Giorgetta (2006), Propagation of ENSO temperature signals into the middle atmosphere: A comparison of two general circulation models and ERA-40 reanalysis data, *J. Geophys. Res.*, *111*, D06101, doi:10.1029/2005JD006061.
- Gill, A. E. (1980), Some simple solutions for heat-induced tropical circulation, *Q. J. R. Meteorol. Soc.*, *106*, 447–462, doi:10.1002/qj.49710644905.
- Highwood, E. J., and B. J. Hoskins (1998), The tropical tropopause, *Q. J. R. Meteorol. Soc.*, *124*(549), 1579–1604, doi:10.1002/qj.49712454911.
- Ho, S.-P., X. Zhou, Y.-H. Kuo, D. Hunt, and J.-H. Wang (2010), Global evaluation of radiosonde water vapor systematic biases using GPS radio occultation from COSMIC and ECMWF analysis, *Remote Sens.*, *2*, 1320–1330, doi:10.3390/RS2051320.
- Holloway, C. E., and J. D. Neelin (2007), The convective cold top and quasi equilibrium, *J. Atmos. Sci.*, *64*, 1467–1487.
- Lau, K.-M., C.-H. Ho, and I.-S. Kang (1998), Anomalous atmospheric hydrologic processes associated with ENSO: Mechanisms of hydrologic cycle-radiation interaction, *J. Clim.*, *11*, 800–815.
- Lu, J., G. Chen, and D. M. W. Frierson (2008), Response of the zonal mean atmospheric circulation to El Niño versus global warming, *J. Clim.*, *21*, 5835–5851, doi:10.1175/2008JCLI2200.1.
- Oort, A. H., and J. J. Yienger (1996), Observed interannual variability in the Hadley circulation and its connection to ENSO, *J. Clim.*, *9*(11), 2751–2767.
- Randel, W. J., F. Wu, and D. J. Gaffen (2000), Interannual variability of the tropical tropopause derived from radiosonde data and NCEP reanalyses, *J. Geophys. Res.*, *105*(D12), 15,509–15,523.
- Randel, W. J., R. R. Garcia, N. Calvo, and D. Marsh (2009), ENSO influence on zonal mean temperature and ozone in the tropical lower stratosphere, *Geophys. Res. Lett.*, *36*, L15822, doi:10.1029/2009GL039343.
- Ryu, J.-H., S. Lee, and S.-W. Son (2008), Vertically propagating Kelvin waves and tropical tropopause variability, *J. Atmos. Sci.*, *65*, 1817–1837, doi:10.1175/2007JAS2466.1.
- Seager, R., N. Harnik, Y. Kushnir, W. Robinson, and J. Miller (2003), Mechanisms of hemispherically symmetric climate variability, *J. Clim.*, *16*(18), 2960–2978.
- Steiner, A. K., B. C. Lackner, F. Ladstädter, B. Scherllin-Pirscher, U. Foelsche, and G. Kirchengast (2011), GPS radio occultation for climate monitoring and change detection, *Radio Sci.*, *46*, RS0D24, doi:10.1029/2010RS004614.
- Su, H., J. D. Neelin, and J. E. Meyerson (2005), Mechanisms for lagged atmospheric response to ENSO SST forcing, *J. Clim.*, *18*, 4195–4215.
- Trenberth, K. E., and L. Smith (2006), The vertical structure of temperature in the tropics: Different flavors of El Niño, *J. Clim.*, *19*, 4956–4973.
- Trenberth, K. E., and L. Smith (2009), Variations in the three-dimensional structure of the atmospheric circulation with different flavors of El Niño, *J. Clim.*, *22*, 2978–2991.
- Wallace, J. M., R. Lee Panetta, and J. Estberg (1993), Representation of the equatorial stratospheric Quasi-Biennial Oscillation in EOF phase space, *J. Atmos. Sci.*, *50*(12), 1751–1762.
- Yulaeva, E., and J. M. Wallace (1994), The signature of ENSO in global temperature and precipitation fields derived from the microwave sounding unit, *J. Clim.*, *7*(11), 1719–1736.
- Zhou, T., and J. Zhang (2011), The vertical structures of atmospheric temperature anomalies associated with two flavors of El Niño simulated by AMIP II models, *J. Clim.*, *24*, 1053–1070, doi:10.1175/2010JCLI3504.1.